Available online at www.sciencedirect.com
SCIENCE DIRECT®
Journal of Sound and Vibration 271 (2004) 241–255
JOURNAL OF SOUND AND VIBRATION
www.elsevier.com/locate/jsvi

A note on a plate having a circular cavity excited by plane harmonic SH waves

A. Hayir*, I. Bakirtas

Civil Engineering Department, Istanbul Technical University, Civil Engineering Department, Division of Mechanics, 34469 Maslak, Istanbul, Turkey

Received 23 July 2002; accepted 13 February 2003

Abstract

A solution for the plate having a circular cavity subject to plane harmonic SH waves, horizontally polarized shear waves, is presented in this paper. The method of solution involves series expansion of incident and reflected SH waves from the cavity and two free surfaces in terms of cylindrical wave functions and the image method, respectively. The image method proposed in this article is used to satisfy the boundary condition of the traction free surfaces on the plate. Then, the boundary condition of the cavity is applied to the solution having unknown coefficients. In order to simplify the problem, only the lowest mode is taken into account in the plate. The results obtained in this study provide important information about the behaviour of the plate near the discontinuity. Numerical results show that the distance between the upper surface and the nearest cavity boundary (at $\theta = 0$, $r = a$) has primary effect. If the radius of the cavity is relatively small compared with the thickness of the plate, the solutions approach the full space's solutions for the cavity, well-known in literature. Also, those solutions for the plate correspond to the solutions of the plate without cavity. Dynamic stress concentration factors around the cavity and displacements in the cross-section of the plate are obtained near the cavity for various wave numbers. It is concluded that the presented solutions are partially analytical solutions, so they can be used for construction and verification of approximate numerical techniques such as the boundary element method (BEM), finite element method (FEM), finite difference method (FDM), etc.

1. Introduction

It is very important to determine the service life of the members of the structure such as beams, columns, plates, shells, etc. They start to loose their strength in time depending on the

*Corresponding author. Tel.: +90-212-285-37-08; fax: +90-212-285-65-87.
E-mail address: ahayir@itu.edu.tr (A. Hayir).

0022-460X/$ - see front matter © 2003 Elsevier Ltd. All rights reserved.
doi:10.1016/S0022-460X(03)00751-X

environmental conditions and external loads. Some failures such as holes and cracks can also occur inside the plate during the construction and loading, and these failures make the structure weak. If a plate has discontinuities such as inclusions like rivets, cavities or cracks, it is definitely vital to determine them and their effects. The stresses and displacements around and near the discontinuities are very different from the design stresses and displacements. Therefore, it is essential that they must be determined in case of dead loads, live loads, internal loads, seismic waves, etc.

Most of the analyses in the literature are made for arbitrary shape discontinuities using numerical methods [1]. Although these numerical methods are very useful tools for these kind of problems, it is very important to determine the physical behaviour of the problem with analytical method. Therefore, the aim of this paper is to give a partially analytical study for the plate having a circular cavity excited by seismic SH waves, horizontally polarized shear waves, and to obtain dynamic stress concentration factors around the cavity and the displacements in the cross-section of the plate for the first mode. In the previous studies, similar solutions are obtained for the plate and the half-space. The solutions of the plate having circular and arbitrary cavities using the analytical and the numerical method are discussed [2–4], and the solutions of the half-space for response of tunnels to incident SH waves [5] and diffraction of SH waves by subsurface inclusions of arbitrary shape [6] are presented.

2. The model and formulation of the problem

The time harmonic SH waves propagating in an infinite plate of thickness H, having shear modulus μ and density ρ are considered. The plate occupies the region $-\infty<(x,z)<\infty, -h_2<y<h_1$ and contains a circular cavity (Fig. 1), where a is the radius of the circular cavity, h_1 and h_2 are the ordinates of the upper surface, and the bottom surface, respectively. $w(x,y)$ is the wave amplitude in the z direction. Two co-ordinate systems are required: A plane cartesian co-ordinate system and a plane polar co-ordinate system as shown in Fig. 1. The z-axis may be assumed to be perpendicular to the plane defined by the two co-ordinate systems.

The excitation in a plate of finite thickness in the case of harmonic SH waves is expressed as shown below [7, p. 205]

$$w^{(i)} = f(y)\exp(\mathrm{i}kx - \mathrm{i}\omega t), \tag{1}$$

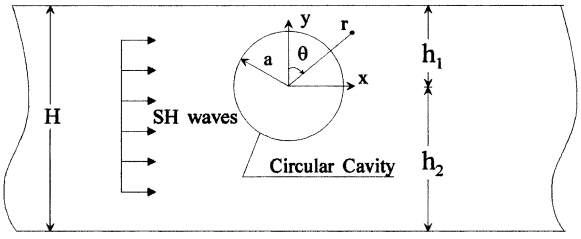

Fig. 1. SH waves in a layer having a circular cavity.

where $w^{(i)}$, k and ω show incident waves, wave number and angular frequency, respectively. This solution must satisfy the following equation:

$$\frac{\partial^2 w}{\partial x^2}+\frac{\partial^2 w}{\partial y^2}=\frac{1}{c_2^2}\frac{\partial^2 w}{\partial t^2}, \tag{2}$$

where $c_2=\sqrt{\mu/\rho}$ is the shear wave velocity. The boundary conditions at $y=h_1,-h_2$ are

$$\sigma_{yz}=\mu\frac{\partial w}{\partial y}=0. \tag{3}$$

Substituting Eq. (1) into Eq. (2), $f(y)$ is found as

$$f(y)=w_0\cos(qy)+w_1\sin(qy), \tag{4}$$

where

$$q^2=\frac{\omega^2}{c_2^2}-k^2. \tag{5}$$

The boundary conditions (3) yield

$$\frac{\omega^2}{c_2^2}-k^2=\left(\frac{n\pi}{h_1+h_2}\right)^2. \tag{6}$$

This result shows that except for $n=0$, the phase velocity depends on the wave number k. Thus harmonic SH waves in an elastic layer are dispersive.

The harmonic incident waves of constant amplitude corresponding to the lowest mode ($n=0$) are considered, but the other modes might be taken into account too. A harmonic incident wave of constant amplitude can be constructed by the help of a source far enough away.

In the case of $n=0$, Eq. (1) can be written as

$$w^{(i)}=w_0\exp(\mathrm{i}kx-\mathrm{i}\omega t), \tag{7}$$

where w_0 is the constant amplitude as shown in Fig 2. In the polar co-ordinates, Eq. (7) may be rewritten as follows:

$$w^{(i)}=w_0\exp\left[\mathrm{i}kr\cos\left(\theta-\frac{\pi}{2}\right)-\mathrm{i}\omega t\right]. \tag{8}$$

In polar co-ordinate, the governing equation is

$$\frac{\partial^2 w}{\partial r^2}+\frac{1}{r}\frac{\partial w}{\partial r}+\frac{1}{r^2}\frac{\partial^2 w}{\partial\theta^2}=\frac{1}{c_2^2}\frac{\partial^2 w}{\partial t^2}. \tag{9}$$

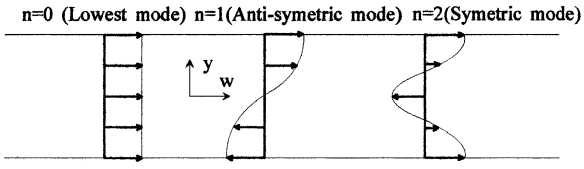

Fig. 2. Displacement distributions in the plate without the cavity for the first, second and third mode in $y-w$ plane.

The boundary condition on the cavity is

$$\sigma_{rz} = \mu \frac{\partial w}{\partial r} = 0, \tag{10}$$

at $r = a$.

Due to the cavity, incident waves, $w^{(i)}$, are scattered by the cavity, the first scattered waves, $w^{(s)}$, are reflected by two surfaces, and the reflected waves, $w^{(sr)}$, are infinitely scattered and reflected many times by the cavity and the surfaces. The total displacement can be written as the sum of incident waves, scattered waves and scattered-reflected waves due to the superposition principle

$$w = w^{(i)} + w^{(s)} + w^{(sr)}. \tag{11}$$

The solution of the first scattered waves by the cavity can be obtained as shown, using the wave expansion method from Eq. (9) [5,6]

$$w^{(s)} = w_0 \sum_{m=0}^{\infty} \mathrm{H}_m^{(1)}(kr)(A_m \cos m\theta + B_m \sin m\theta), \tag{12}$$

where $w^{(s)}$, $\mathrm{H}_m^{(1)}$, A_m and B_m represent outgoing scattered waves satisfying Sommerfield radiation condition, first type Hankel function and unknown coefficients, respectively. The time factor, $\exp(-\mathrm{i}\omega t)$, is implied and omitted in this and later formulations.

The solution of the scattered-reflected waves are naturally similar to the scattered waves. The surface boundary conditions in Eq. (3) are satisfied using the image method [7, p. 113].

The idea of the imaging primary cavity, which corresponds to the source, with respect to the traction free surfaces can also be used to determine the Green's function for a region bounded by two planes. In this case we take the image of the primary cavity with respect to both $y = h_1$ and $y = -h_2$. The image with respect to $y = -h_2$ destroys, however, the symmetry of the primary cavity and its image with respect to $y = h_1$, and thus another cavity must be added in the region $y > h_1$ to restore symmetry. The system of cavities must, however, also again be symmetric with respect to $y = -h_2$, which establishes the need for another cavity at $y < -h_2$, whereupon an additional source must be applied at $y > h_1$, and so forth. The co-ordinate systems are in the opposite direction to keep the symmetry with respect to the surface of the plate in every second image cavity. It is concluded that an infinite number of cavities is needed to satisfy the conditions of Eq. (3). At a point $-h_2 < y < h_1$, an infinite sequence of waves is observed. The waves, ($w^{(s)}$ and $w^{(sr)}$) are interpreted as the scattered waves and the subsequent reflections from the free surfaces. The cavities and the pattern of the waves are shown in Fig. 3.

Ultimately, there is a solution in the form of a series: For the image cavities,
In the upper side of the plate for the first image cavity

$$w^{(s_1)}(r_1, \theta_1) = w_0 \sum_{m=0}^{\infty} \mathrm{H}_m^{(1)}(kr_1)(A_m \cos m\theta_1 + B_m \sin m\theta_1). \tag{13a}$$

In the lower side of the plate for the first image cavity

$$w^{(s_1*)}(r_{1*}, \theta_{1*}) = w_0 \sum_{m=0}^{\infty} \mathrm{H}_m^{(1)}(kr_{1*})\,(A_m \cos m\theta_{1*} + B_m \sin m\theta_{1*}). \tag{13b}$$

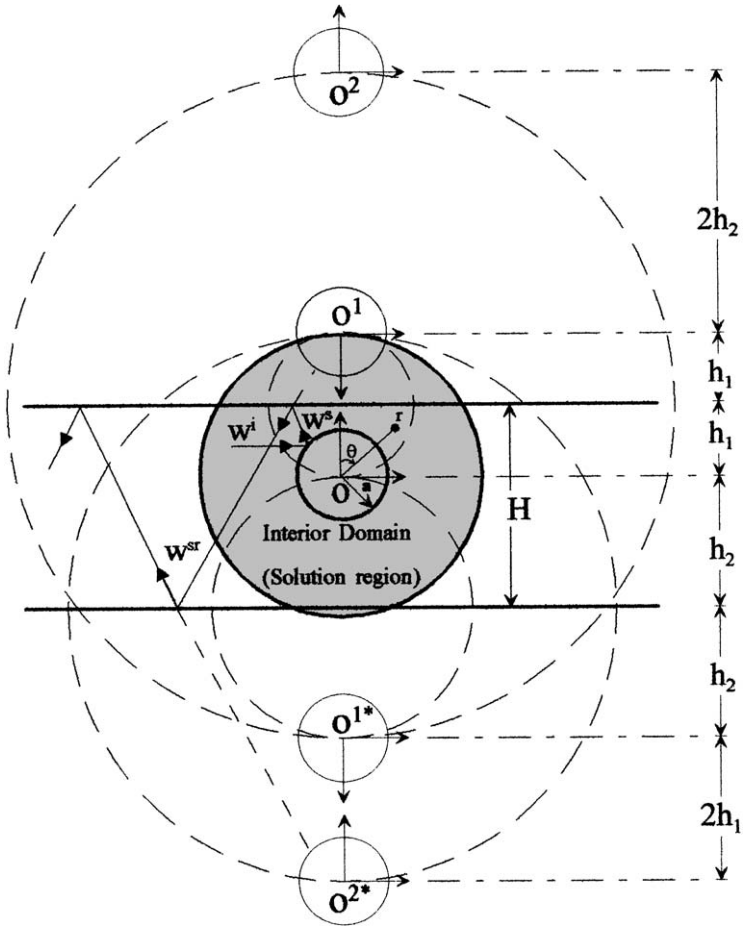

Fig. 3. Application of the image method in the plate for SH waves.

In the upper side of the plate for the second image cavity

$$w^{(s_2)}(r_2,\theta_2) = w_0 \sum_{m=0}^{\infty} \mathrm{H}_m^{(1)}(kr_2)\,(A_m \cos m\theta_2 + B_m \sin m\theta_2). \tag{13c}$$

In the lower side of the plate for the second image cavity

$$\begin{aligned} w^{(s_2*)}(r_{2*},\theta_{2*}) &= w_0 \textstyle\sum_{m=0}^{\infty} \mathrm{H}_m^{(1)}(kr_{2*})\ (A_m \cos m\theta_{2*} + B_m \sin m\theta_{2*}). \\ &\vdots \end{aligned} \tag{13d}$$

As a result, these solutions can be written in the series form:
In the upper side of the plate

$$w^{(sr)}(r_d,\theta_d) = w_0 \sum_{m=0}^{\infty} \sum_{d=0}^{\infty} \mathrm{H}_m^{(1)}(kr_d)\,(A_m \cos m\theta_d + B_m \sin m\theta_d). \tag{14a}$$

Likewise, in the lower side of the plate

$$w^{(sr)}(r_{d*},\theta_{d*}) = w_0 \sum_{m=0}^{\infty} \sum_{d*=0}^{\infty} \mathrm{H}_m^{(1)}(kr_{d*})\,(A_m \cos m\theta_{d*} + B_m \sin m\theta_{d*}), \tag{14b}$$

where d and d^* represent the series index representing the image cavities. $w^{(sr)}(r_d,\theta_d)$ and $w^{(sr)}(r_{d*},\theta_{d*})$ correspond to the outgoing scattered waves satisfying Sommerfield radiation condition for image cavities.

Amplitude functions given by Eqs. (14a), (14b) in terms of polar co-ordinates (r_d,θ_d) and (r_{d*},θ_{d*}) differ from each other. Using the Graf's addition theorem [8–11] in the interior regions for image cavities, the solution of the scattered-reflected waves in terms of (r,θ) is given by

$$w^{(sr)} = w_0 \sum_{m=0}^{\infty} \sum_{d=1}^{\infty} \mathrm{J}_m(kr)[(A_{md}^U + A_{md}^L)\cos m\theta + (B_{md}^U + B_{md}^L)\sin m\theta], \tag{15}$$

where A_{md}^U, A_{md}^L, B_{md}^U and A_{md}^L are related to $\mathrm{P}_{mn}^{\pm}(C_1)$, A_m and B_m.

For $m = 0, 1, 2, \ldots$, and $d = 1, 3, 5, \ldots$,

$$\begin{aligned}
A_{md}^U &= \sum_{n=0}^{\infty} \mathrm{P}_{mn}^{+}[k(p\,H + 2h_1)]A_n,\\
A_{md}^L &= \sum_{n=0}^{\infty} (-1)^{n+m}\,\mathrm{P}_{mn}^{+}[k(pH + 2h_2)]A_n,\\
B_{md}^U &= \sum_{n=0}^{\infty} \mathrm{P}_{mn}^{-}[k(pH + 2h_1)]B_n,\\
B_{md}^L &= \sum_{n=0}^{\infty} (-1)^{n+m}\,\mathrm{P}_{mn}^{-}[k(pH + 2h_2)]B_n,
\end{aligned} \tag{16a}$$

where d represents the indices for the image cavities, and $p = d - 1$, for $m = 0, 1, 2, \ldots$, and $d = 2, 4, 6, \ldots$,

$$\begin{aligned}
A_{md}^U &= \sum_{n=0}^{\infty} (-1)^{n}\,\mathrm{P}_{mn}^{+}[dkH]A_n,\\
A_{md}^L &= \sum_{n=0}^{\infty} (-1)^{m}\,\mathrm{P}_{mn}^{+}[dkH]A_n,\\
B_{md}^U &= \sum_{n=0}^{\infty} (-1)^{n+1}\,\mathrm{P}_{mn}^{-}[dkH]B_n,\\
B_{md}^L &= \sum_{n=0}^{\infty} (-1)^{m+1}\,\mathrm{P}_{mn}^{-}[dkH]B_n
\end{aligned} \tag{16b}$$

and

$$\mathrm{P}_{mn}^{\pm}(C_1) = \frac{\varepsilon_m}{2}\left[\mathrm{H}_{n+m}^{(1)}(C_1) \pm (-1)^m \mathrm{H}_{n-m}^{(1)}(C_1)\right], \tag{17}$$

where $m = 0, 1, 2, \ldots$, and $n = 0, 1, 2, \ldots$, $\varepsilon_0 = 1$, $m \geqslant 1$ $\varepsilon_m = 2$, and C_1 represents the argument.

The incident waves for combining with scattered waves and scattered-reflected waves are written in terms of cosine series

$$w^i = w_0 \sum_{m=0}^{\infty} \varepsilon_m \mathrm{i}^m \mathrm{J}_m(kr) \left[\cos m\theta \cos\frac{m\pi}{2} + \sin\frac{m\pi}{2} \sin m\theta\right], \tag{18}$$

where $\varepsilon_0 = 1$, $m \geqslant 1$, $\varepsilon_m = 2$.

For the final case, the whole displacement field is

$$w = w_0 \left(\sum_{m=0}^{\infty} \varepsilon_m \mathrm{i}^m \mathrm{J}_m(kr) \left[\cos m\theta \cos\frac{m\pi}{2} + \sin\frac{m\pi}{2} \sin m\theta\right] + \sum_{m=0}^{\infty} \left[\mathrm{H}_m^{(1)}(kr)[A_m \cos m\theta + B_m \sin m\theta] + \mathrm{J}_m(kr) \sum_{d=1}^{\infty} \left[(A_{md}^U + A_{md}^L)\cos m\theta + (B_{md}^U + B_{md}^L)\sin m\theta\right] \right] \right). \tag{19}$$

With the substitution of Eq. (19) into Eq. (10), the following equations are obtained:

$$\left.\frac{\partial \mathrm{H}_m^{(1)}(kr) A_m}{\partial r}\right|_{r=a} + \frac{\partial \mathrm{J}_m(kr)}{\partial r} \sum_{d=1}^{\infty} (A_{md}^U + A_{md}^L)_{r=a} = -\varepsilon_m \mathrm{i}^m \cos\frac{m\pi}{2} \left.\frac{\partial \mathrm{J}_m(kr)}{\partial r}\right|_{r=a}, \tag{20a}$$

$$\left.\frac{\partial \mathrm{H}_m^{(1)}(kr) B_m}{\partial r}\right|_{r=a} + \frac{\partial \mathrm{J}_m(kr)}{\partial r} \sum_{d=1}^{\infty} (B_{md}^U + B_{md}^L)_{r=a} = -\varepsilon_m \mathrm{i}^m \sin\frac{m\pi}{2} \left.\frac{\partial \mathrm{J}_m(kr)}{\partial r}\right|_{r=a}. \tag{20b}$$

The constant coefficients A_m and B_m are determined by solving these two equations. When these coefficients are substituted into Eq. (19), total displacement field is determined.

3. Accuracy of the results

Numerical results are presented for the dimensionless absolute stresses and displacements in the vertical cross-sections, and dynamic stress concentration factors, where σ_0, M, N, η and D represent the absolute value of the plate for the first mode without the cavity, maximum number of the series, dimensionless frequency and the maximum number of the image cavities, respectively. It is very difficult, sometimes even impossible to prove the convergence of the double Bessel series. So, in this study, all presented numerical results are controlled by the boundary conditions, which are satisfied approximately. For this purpose some examples are presented in Figs. 4a–d. They show the accuracy of the solution for certain given parameters. Even if the figures do not prove the convergence of the solution, the numerical results show that the boundary condition on the plate is nearly satisfied according to the number of the cavities. The effects of the image cavities on the real cavity and in its vicinity decrease depending on the distances between the real cavity and the image cavities because of the attenuation of the elastic waves.

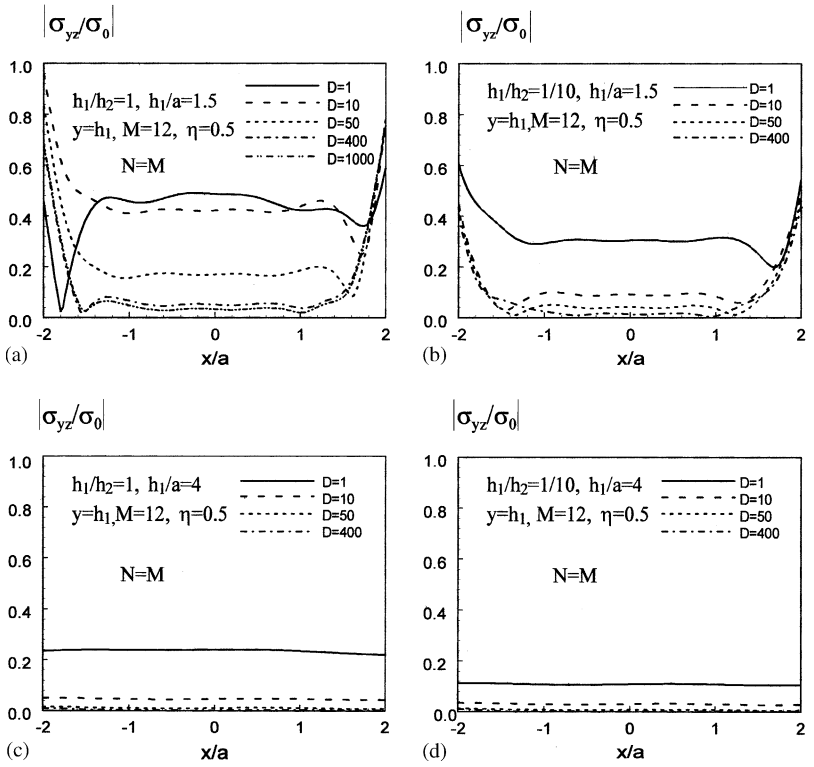

Fig. 4. (a–d) Dimensionless absolute stresses, $|\sigma_{yz}/\sigma_0|$, on the upper free surface versus x/a.

4. Numerical results

Numerical results are illustrated in the vicinity of the cavity, i.e., in the interior region. In fact this region is much more significant than farther regions from the cavity, since maximum stresses and displacements occur in this region depending on the cavity.

For the numerical examples, a set of discrete dimensionless frequency, η, is defined as [6]

$$\eta = \frac{ka}{\pi} = \frac{\omega a}{\pi c_2}, \tag{21}$$

where η is the dimensionless frequency.

Fig. 5a and b illustrates dimensionless absolute stresses, $|\sigma_{yz}/\sigma_0|$, versus y/a from 0 to h_1/a at $x/a = -1.5$, 0 and 1.5 for $h_1/a = 1.5$ and 4 in case of $h_1/h_2 = 1$, $M = N = 12$, $D = 1000$ and $\eta = 0.5$; $h_1/h_2 = 1/10$, $M = N = 12$, $D = 400$ and $\eta = 0.5$; $h_1/h_2 = 1$, $M = N = 22$, $D = 1000$, $\eta = 1$; $h_1/h_2 = 1/10$, $M = N = 22$, $D = 400$ and $\eta = 1$; and the first mode solution of the plate. The stresses are slightly smaller in the shadow side, at $x/a = 1.5$, than that on the illuminated side, at $x/a = -1.5$. It can be seen also from the figures that stresses in the boundaries are almost zero. Also the results depict that the stresses in this direction would be zero if the cavity was not there. Fig. 6a and b shows dimensionless absolute displacements, $|w/w_0|$, versus y/a from 0 to h_1/a at

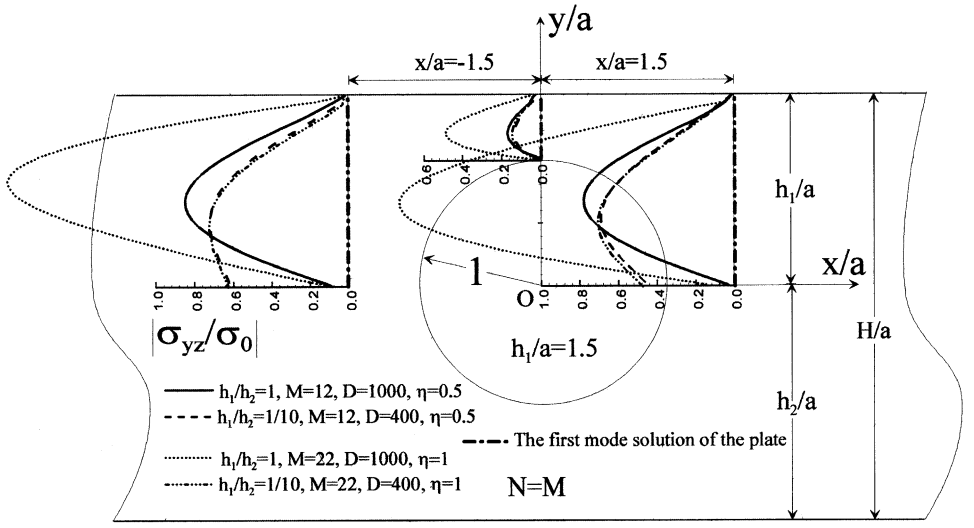

(a)

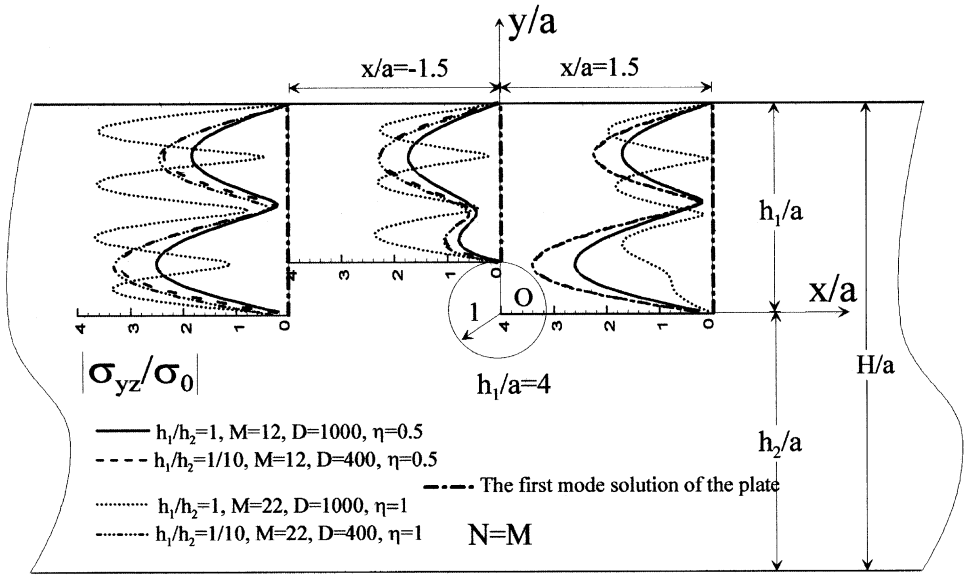

(b)

Fig. 5. Dimensionless absolute stresses, $|\sigma_{yz}/\sigma_0|$, versus y/a from 0 to h_1/a at $x/a = -1.5$, 0 and 1.5 for (a) $h_1/a = 1.5$ and (b) $h_1/a = 4$.

$x/a = -1.5$, 0 and 1.5 for $h_1/a = 1.5$ in case of $h_1/h_2 = 1$, $M = N = 12$, $D = 1000$ and $\eta = 0.5$; $h_1/h_2 = 1/10$, $M = N = 12$, $D = 400$ and $\eta = 0.5$; $h_1/h_2 = 1$, $M = N = 22$, $D = 1000$, $\eta = 1$; $h_1/h_2 = 1/10$, $M = N = 22$, $D = 400$ and $\eta = 1$; and the first mode solution of the plate. It can be seen from the figures that the displacements fluctuate near the one representing the first mode solutions of the plate except for the cavity.

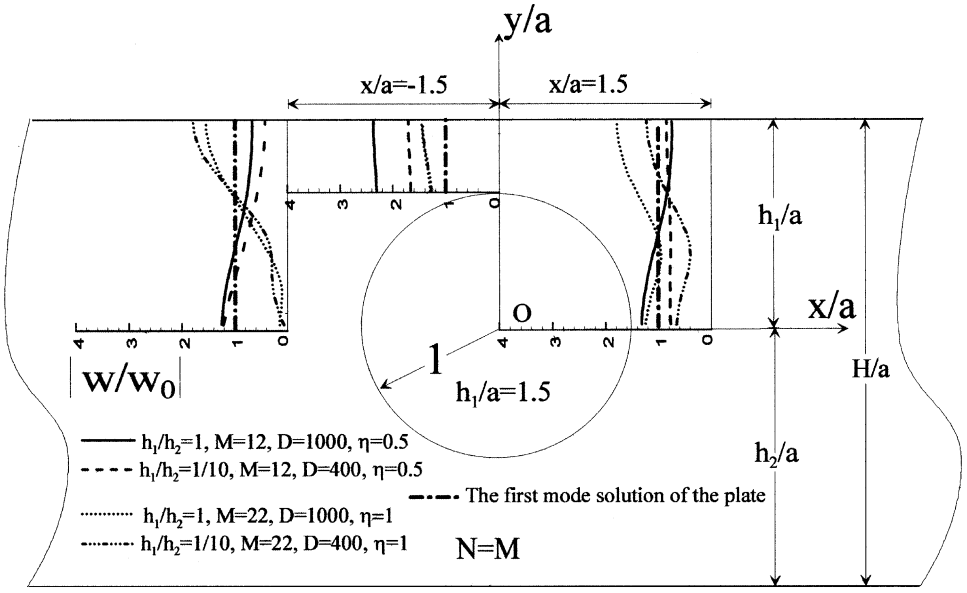

(a)

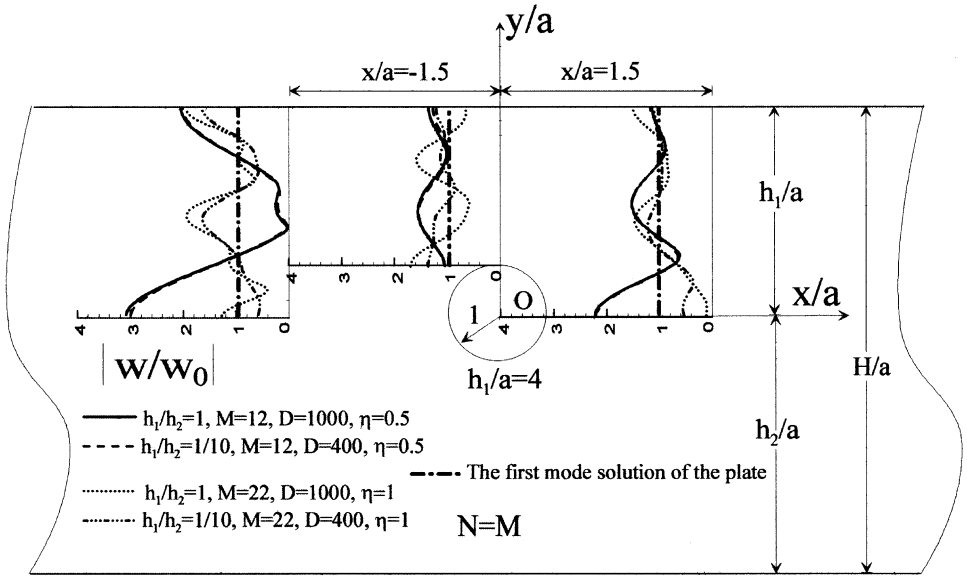

(b)

Fig. 6. Dimensionless absolute displacements, $|w/w_0|$, versus y/a from 0 to h_1/a at $x/a = -1.5$, 0 and 1.5 (a) $h_1/a = 1.5$ and (b) $h_1/a = 4$.

Without the cavity, absolute value of the stresses for incident waves in the x direction in the plate for the first mode solution [12, p. 132] is

$$\sigma_0 = w_0 \mu k, \tag{22}$$

and with the cavity, the stress around the cavity is

$$\sigma_{\theta z} = -\sigma_0 \frac{1}{ka}\left\{\sum_{m=0}^{\infty} m\varepsilon_m i^m \mathrm{J}_m(ka)\sin m\left(\theta-\frac{\pi}{2}\right)+\sum_{m=0}^{\infty} m\left[\mathrm{H}_m^{(1)}(ka)(A_m \sin m\theta - B_m \cos m\theta)+\mathrm{J}_m(ka)\sum_{d=1}^{\infty}[(A_{md}^U + A_{md}^L)\sin m\theta-(B_{md}^U + B_{md}^L)\cos m\theta]\right]\right\}. \quad (23)$$

Fig. 7 shows a comparison of dynamic stress concentration factors, $|\sigma_{\theta z}/\sigma_0$, around the cavity between the full-space (for which $ka = 0.1, 1$ and 2 and $M = 10$) and the plate (for which $ka = 0.1$, $M = N = 8$ and $D = 400$; $ka = 1$, $M = N = 10$ and $D = 400$; $ka = 2$, $M = N = 12$ and $D = 400$) for $h_1/h_2 = 1$ and $h_1/a = 1.5$. They are all symmetric with respect to horizontal axis, x, and the fluctuation starts as ka increases. When $ka = 0.1$, the angular distribution is nearly the same as for the static value which can be obtained $ka \to 0$ and is symmetric for both axes. However, the values of concentration factor for $ka = 1$ is higher on the illuminated side than on the shadow side for the full-space contrary to the results of the plate. The values of the concentration factor for $ka = 2$ for both full-space [12, p. 134] and the plate are higher on the shadow side than on the illuminated side.

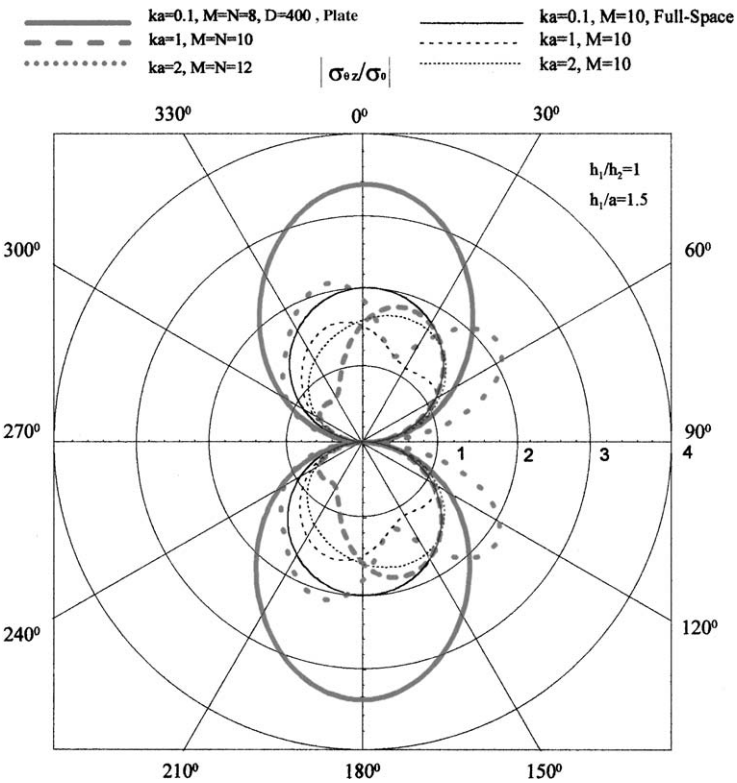

Fig. 7. Comparison of the dynamic stress concentration factors, $|\sigma_{\theta z}/\sigma_0|$, around the cavity for $h_1/h_2 = 1$ and $h_1/a = 1.5$.

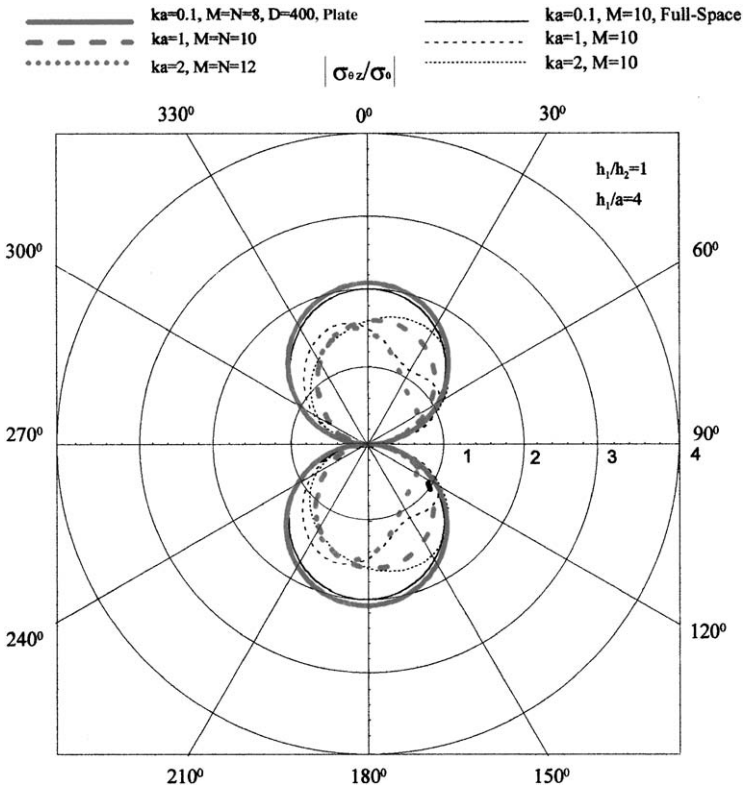

Fig. 8. Comparison of the dynamic stress concentration factors, $|\sigma_{\theta z}/\sigma_0|$, around the cavity for $h_1/h_2 = 1$ and $h_1/a = 4$.

Fig. 8 shows comparison of dynamic stress concentration factors, $|\sigma_{\theta z}/\sigma_0|$, around the cavity between the full-space (for which $ka = 0.1$, 1 and 2, and $M = 10$ and the plate (for which $ka = 0.1, M = N = 8$ and $D = 400$; $ka = 1$, $M = N = 10$, $D = 400$; and $ka = 2$, $M = N = 12$ and $D = 400$) for $h_1/h_2 = 1$ and $h_1/a = 1.5$. When $ka = 0.1$, the angular distribution is nearly the same for the static value and symmetric for both axes. The concentration factors for both the full-space and the plate are slightly different from each other. The values of the concentration factor for $ka = 1$ is smaller on the illuminated side than on the shadow side for the plate contrary to full-space results. The values of the concentration factor for $ka = 2$ are higher on the illuminated side than on the shadow side for the plate contrary to the full-space results.

Fig. 9 shows comparison of dynamic stress concentration factors, $|\sigma_{\theta z}/\sigma_0|$, around the cavity between the full-space (for which $ka = 0.1$, 1 and 2, and $M = 10$) and the plate (for which $ka = 0.1$, $M = N = 8$ and $D = 400$; $ka = 1, M = N = 10$, $D = 400$; and $ka = 2$, $M = N = 12$ and $D = 400$) for $h_1/h_2 = 1$ and $h_1/a = 4$. When $ka = 0.1$, the angular distribution is nearly the same for static value. The concentration factors are bigger at $90^\circ \leqslant \theta \leqslant 270^\circ$ than on the other side (upper side) for the plate. In the upper side, the values of the concentration factor of the plate for $ka = 2$ are higher on the shadow side than on the illuminated side such as the results of the

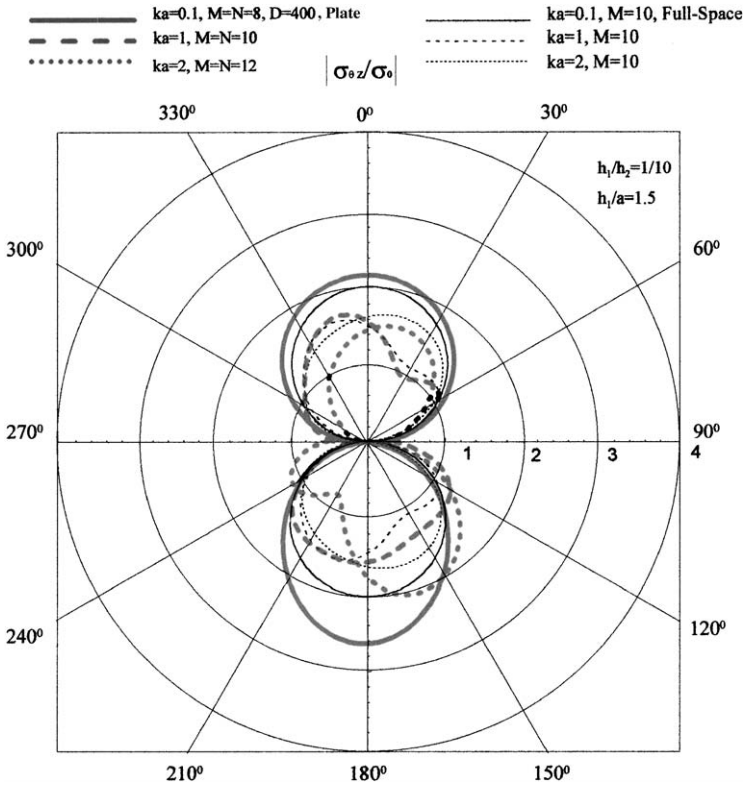

Fig. 9. Comparison of the dynamic stress concentration factors, $|\sigma_{\theta z}/\sigma_0|$, around the cavity between the full-space (for which $ka = 0.1$, 1, and 2, and $M = 10$) and the plate (for which $ka = 0.1$, $M = N = 8$ and $D = 400$; $ka = 1$, $M = N = 10$, $D = 400$; and $ka = 2$, $M = N = 12$ and $D = 400$) for $h_1/h_2 = 1/10$ and $h_1/a = 4$.

full-space. In the lower side, the concentration factors of the plate for $ka = 1$ and 2 are higher on the shadow side than on the illuminated side.

Fig. 10 depicts dynamics stress concentration factors at $r = a$, $\theta = 0$ $(h_1/h_2 = 1)$ versus dimensionless wave numbers, ka, for $h_1/a = 1.5$, 4 and full-space. The results show that when ka increases, the values of the dynamic stress concentration are approaching each other for both full-space and the plate.

5. Conclusions

The purpose of this study is to obtain some numerical results for the plate having circular cavity exited by plane harmonic SH waves, well-known in literature. The numerical results are partially analytic, so they may guide the results of numerical methods such as BEM, FEM, FDM, etc. These results might help to solve and understand more complicated problems which are important in engineering and applied sciences.

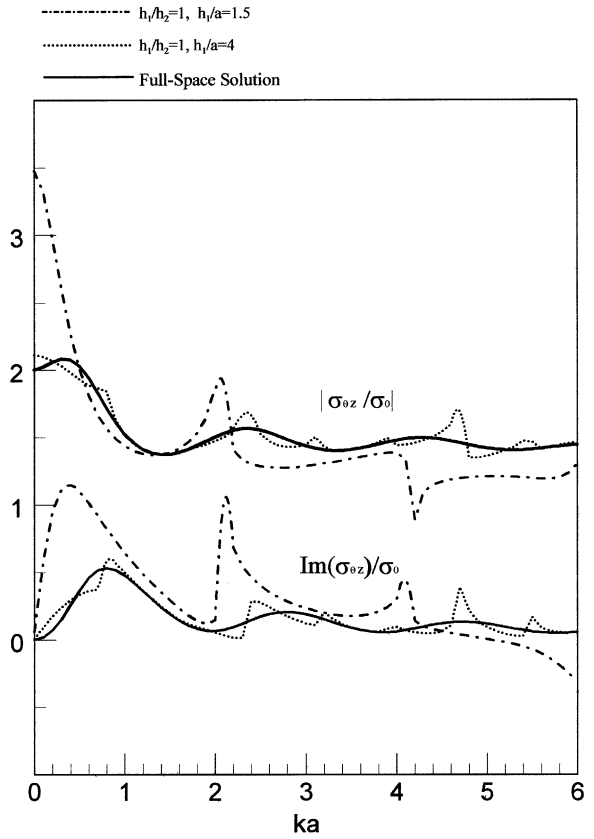

Fig. 10. Dynamics stress concentration factors, $|\sigma_{\theta z}/\sigma_0|$, at $r = a$, $\theta = 0$ ($h_1/h_2 = 1$) (versus dimensionless wave numbers ka for $h_1/a = 1.5$, 4 and full-space.

Acknowledgements

The work conducted here was supported by the Institute of Science and Technology, Istanbul Technical University. The authors thank H. Kerem Cigizoglu for his critical reading of the manuscript.

References

[1] M.R. Karim, M.A. Awal, T. Kundu, Numerical-analysis of guided wave scattering by multiple cracks in plates SH-case, *Engineering Fracture Mechanics* 42 (2) (1992) 371–380.

[2] A. Hayir, Scattering of SH Waves by Arbitrary Cavities of Arbitrary Shape in a Waveguide, Ph.D. Dissertation, Istanbul Technical University, Istanbul, 1998 (in Turkish).

[3] A. Hayir, I. Bakirtas, Dynamic stress concentration factors around the elliptical cavities in a waveguide-SH case, *1st International Symposium on Mechanical Vibration*, Islamabad, Pakistan, 1998, pp. 64–79.

[4] A. Hayir, I. Bakirtas, Scattering of SH waves by cavities of arbitrary shape in a waveguide, *13th ASCE EMD*, Baltimore, MD, 1999.

[5] V.W. Lee, M.D. Trifunac, Response of tunnels to incident Sh-waves, *Engineering Mechanics Division American Society of Civil Engineers* 105 (1979) 643–659.
[6] M.E. Manoogian, V.W. Lee, Diffraction of Sh-waves by subsurface inclusions of arbitrary shape, *Engineering Mechanics Division American Society of Civil Engineers* 122 (1996) 123–129.
[7] J.D. Achenbach, *Wave Propagation in Elastic Solids*, North-Holland, Amsterdam, 1973.
[8] M. Abramowitz, I.A. Stegun, *Handbook of Mathematical Function*, Dover, New York, 1975.
[9] A. Hayir, M.I. Todorovska, M.D. Trifunac, Antiplane response of a dike with flexible soil–structure interface to incident SH-waves, *Soil Dynamics and Earthquake Engineering* 21 (2001) 603–613.
[10] M.I. Todorovska, A. Hayir, M.D. Trifunac, Antiplane response of a dike on flexible embedded foundation to incident SH-waves, *Soil Dynamics and Earthquake Engineering* 21 (2001) 593–601.
[11] X. Yuan, Z.P. Liao, Scattering of plane SH waves by a cylindrical alluvial of circular-arc cross-section, *Earthquake Engineering and Structural Dynamics* 24 (1995) 1303–1313.
[12] Y.H. Pao, C.C. Mow, *Diffraction of Elastic Waves and Dynamics Stress Concentrations*, Crane, Russak and Co., Inc., New York, 1973.